ELSEVIER

International Journal of Mass Spectrometry 226 (2003) 189–209

International Journal of Mass Spectrometry

www.elsevier.com/locate/ijms

Fundamentals of matrix-assisted laser desorption/ionization mass spectrometry with pulsed infrared lasers

Klaus Dreisewerd*, Stefan Berkenkamp, Arne Leisner, Andreas Rohlfing, Christoph Menzel

Institute of Medical Physics and Biophysics, University of Münster, Robert-Koch-Str. 31, D-48149 Münster, Germany

Received 29 August 2001; accepted 10 August 2002

Abstract

The fundamental work and current knowledge on the mechanisms of matrix-assisted laser desorption ionization with pulsed infrared lasers is reviewed and discussed, with a special emphasis on the work performed in the laboratory of the authors in the recent past. The role of the different relevant irradiation parameters (laser wavelength, laser pulse duration, irradiated area and laser fluence) and matrix properties (absorption, state of aggregation) in the MALDI process is summarized as well as results on the dynamic parameters of the expanding desorption plume. New results include an extension of former wavelength studies to the 10 μm wavelength range. Furthermore, a detailed analysis of matrix ion signals generated at infrared laser wavelengths around 3 and 10 μm is presented and compared to those generated by UV-MALDI, revealing a complex picture of the hitherto hardly understood IR-MALDI ionization mechanisms. Preliminary results from a photoacoustic study of the desorption process point to a prolonged material evaporation in case of liquid matrices and pulsed Er:YAG laser excitation. The combined description of the various fundamental work promotes the understanding of the IR-MALDI desorption and ionization processes and allows an assessment of possible solutions for current mass spectrometric limitations of the IR-MALDI method.

Keywords: IR-MALDI; Matrix-assisted laser desorption/ionization; Infrared laser; Glycerol; Photoacoustic

1. Introduction

Whereas, historically, pulsed infrared lasers and in particular pulsed CO_2 lasers were the first with which the analysis of involatile, thermally labile biomolecules by (direct) laser desorption ionization (LDI) mass spectrometry was demonstrated [1], matrix-assisted laser desorption ionization mass spectrometry (MALDI-MS) has since its invention in the mid 1980s [2,3] essentially been associated with the use of pulsed UV-lasers (UV-MALDI-MS). From the potentially useful lasers, mostly pulsed N_2 lasers are employed for UV-MALDI. After a short time of rapid methodological and instrumental development, UV-MALDI-MS has become an established technique for the analysis of a wide range of biomolecules and technical polymers.

First results for MALDI with pulsed infrared (IR) lasers were reported by Overberg et al. in 1990, employing, in a first study, an Er:YAG laser with an emission wavelength of 2.94 μm (pulse duration, ∼200 ns) [4] and, shortly later, a CO_2 laser with an emission wavelength of 10.6 μm (pulse duration, 70 ns) [5].

* Corresponding author.
E-mail address: dreisew@uni-muenster.de (K. Dreisewerd).

1387-3806/02/$ – see front matter
PII S1387-3806(02)00977-6

Over the recent years continuous progress has been achieved in a number of work with respect to both, mechanisms and applications of the method, as will be delineated in this article. In addition to the erbium- and CO_2 lasers, wavelength-tunable optical parametric oscillator (OPO) lasers and a free electron laser (FEL) have been employed in a number of studies with mainly fundamental background.

A critical discussion of the IR-MALDI characteristics with respect to mass spectrometric performance (sensitivity, accuracy/precision, mass resolution, and applicability to different analyte classes) has previously been given by the authors for the 3 and 10 μm wavelength ranges [6,7]. In a general statement and summarizing the present status one could say that IR-MALDI-MS can, in principle, be used for essentially all fields for which UV-MALDI has proven to work. For most of the more widespread applications like the TOF-MS analysis of peptides in, e.g., proteomics, the current UV-MALDI performance is, however, generally not reached.

IR-MALDI has on the other hand been demonstrated to be advantageously implemented whenever particularly large and/or labile compounds have to be analyzed, samples which are frequently not amenable to UV-MALDI analysis at all. Comparing the two, UV and IR wavelength regimes, IR-MALDI is, hence, generally regarded as the softer desorption method and as to lead to a particularly low degree of metastable ion fragmentation. As a result, the generation of intact protein ions with molecular weights exceeding 500 kDa has been demonstrated [6].

Even more pronounced differences between UV- and IR-MALDI are found in the analysis of high molecular weight DNA and RNA samples [8,9]. Employing glycerol as IR matrix, Berkenkamp et al. demonstrated the detection of up to 2180 nt DNA and 1200 nt RNA from samples containing as few as a few hundred attomols [9]. In contrast, the useful mass range for UV-MALDI is currently limited to about 90 nt due to extensive metastable ion fragmentation. Unfortunately, the FWHM mass resolution of the high mass oligonucleotide ion signals generated by IR-MALDI from a glycerol matrix is presently still relatively low and about a few ten only. A number of studies have been performed in the authors' laboratory to elucidate the reasons for these limitations and will be reported in the present publication. For large proteins, mass resolution is generally higher and about 100–200; mass resolution for peptides, finally, is on the order of a few thousand (see below).

In the latter, low to medium mass range, peptides with weakly bound side groups, e.g., phospho- and sialic acid-containing glycopeptides, were recently demonstrated by Cramer et al. to be advantageously analyzed by IR-MALDI [10]. Photosensitive compounds with a high absorption at the wavelength of the common UV-lasers form other, intrinsic examples when IR-MALDI is advantageously applied, as was, for example, reported by Siegel et al. [11].

Because energy deposition proceeds via vibronic modes rather than electronic excitation as in the UV, IR-MALDI also allows the choice from a wider collection of matrix compounds. In particular the use of a number of liquid matrices is possible which barely exist for the UV. One advantage can, for instance, be the use of matrices with pH properties resembling physiological environment conditions of the analyte of interest (e.g., glycerol, Tris–HCl).

An interesting utilization of IR-MALDI from a liquid matrix was recently demonstrated by Lawson and Murray, who coupled capillary electrophoresis (CE) with IR-MALDI-TOF-MS [12]. In this work, ethanol mixed with low concentrations of glycerol was utilized as effluent for the CE system, delivered on-line to a stainless steel frit forming the MALDI target, and finally desorbed/ionized from this frit. Very recently, Twerenbold et al. described a micro-machined silicon injector device with which small droplets of glycerol/analyte solution were injected into the mass spectrometer and deposited directly on the front side of the silicon target holder [13]. A pulsed CO_2 laser was used for desorption/ionization from the small droplets of 4 μm size. Insulin and lysozyme were used as protein samples.

IR-MALDI, on the other hand, is in some respect currently still associated with a few yet to solve drawbacks when compared to the established

UV-MALDI performance. If solid state matrices are used, a major obstacle is, for example, formed by the high sample consumption per laser exposure, which frequently allows only a very limited number of laser exposures per preparation. Previous studies also indicated early on a disadvantageous need for higher concentrated samples, as compared to UV-MALDI requirements [6]. As a result, a lower analytical sensitivity follows for IR-MALDI and (stable) peptides. For peptides, sensitivities in the low femtomole range have thus been demonstrated, which has to be compared to the middle to lower attomol range accessible with UV-MALDI.

Liquid matrices have in many respects proven to form a viable alternative. These matrices have the inherent advantage of providing an intrinsically homogeneous sample morphology and a high shot-to-shot signal stability. In terms of reproducibility they have, in fact been, found to provide a performance very comparable to optimal UV-MALDI [6,9]. Also the "lifetime" of the preparation, i.e., the possible number of laser exposures per preparation, is effectively increased. Among the known liquid IR-matrices, best results have hitherto been obtained with the "FAB-matrix" glycerol. A certain disadvantage in the preparation protocol is the eventual need for cooling of the target because of the relatively high volatility of glycerol.

So far, IR-MALDI has mostly been coupled to axial time-of-flight (TOF) instruments in which ions are extracted in the direction of the initial plume movement. Unfortunately, the use of liquid matrices in combination with these most common instruments is typically accompanied by a significant and for many applications unacceptable reduction in the achievable mass resolution. As is discussed in detail in this publication, the reasons for these problems must be regarded as being essentially process-related. Above all, they are apparently caused by an unfavorable expansion dynamics of the MALDI plume.

Coupling of IR-MALDI sources with alternative analyzers, and in particular the employment of collisional cooling of the plume prior to acceleration in, for instance, orthogonal extraction (o-TOF) instruments, has recently been shown to provide an elegant means of solving the plume dynamics problems while making advantageous use of the soft desorption properties [14,15]. An assessment of the potentials of these instrumental combinations will be given at the end of the present publication.

It should be noted that a wider use of IR-MALDI is at present also hampered by the relatively high costs of potential IR-lasers, considerably exceeding those of the most common N_2-lasers for the UV. To our experience, all currently available IR-lasers, moreover, still exhibit a considerably lower long-term stability and will therefore, in general, require more efforts for maintenance (e.g., readjustment of the laser resonator).

Several groups have in the recent past performed work on different aspects of the desorption/ionization processes. Overall, these studies have revealed a rather complex and sometimes contradictory picture of the IR-MALDI mechanisms. It is the objective of the present publication to outline the essential findings from these studies and in particular extract those relevant for the analytical application of IR-MALDI-MS and potential future methodological and instrumental developments.

This overview will be supplemented by results from recent work from our laboratory. This includes the extension of former wavelength studies in the 2.5–4.0 μm wavelength range (absorption by O–H, N–H, and C–H stretch vibrations [16]) to the 10 μm wavelength range (absorption by O–H bending and C–O stretch vibrations), with a somewhat unexpected result. A detailed comparison of matrix ion signals generated at IR wavelengths in the 3 and 10 μm wavelength range, and with those observed for UV-MALDI revealed a complex picture of the ionization mechanisms. Preliminary results from a photoacoustic study, in which stress waves, generated by the laser–matrix interaction and material ablation, were analyzed, are also presented and allow a temporal analysis of the overall material ablation. Finally, results from recent studies on the dynamics of the IR-MALDI plume expansion will be reported and the associated problems for TOF-MS analysis discussed.

This article is published as part of an honor biography issue of the journal on the occasion of the 65th

birthday of Prof. Franz Hillenkamp, in/under whose laboratory and supervision the described investigations have essentially been carried out. They therefore also reflect a significant part of his scientific work in about the last decade.

2. Experimental

2.1. Mass spectrometer

All experiments were carried out with an in-house built single-stage reflectron time-of-flight mass spectrometer (TOF-MS) of 3.5 m equivalent flight length. The instrument can also be used in the linear TOF mode with a flight length of 2.16 m. Ions were accelerated through a total potential difference of 16–25 kV in a two stage Wiley/McLaren ion extraction source with distances S_1 and S_2 of 6 and 12.5 mm, respectively. Delayed extraction was applied with a maximum switched voltage of 6 kV. Venetian-blind secondary electron multipliers (SEM) (9643/A, Emi-Thorn, Ruislip, UK), equipped with a CuBe conversion dynode, mounted 10 mm in front of the first dynode of the SEM, were used as standard detectors for ion detection. For analytes exceeding 10 kDa the potential between the conversion dynode and the SEM was usually set to −15 kV in order to increase the ion signal by efficient detection of secondary ions, produced at the conversion dynode. Signals were processed by a transient recorder (LeCroy 9350A, Chestnut Ridge, NY, USA) with a maximum time resolution of 2 gigasamples/s, and the digitized data transferred to a PC for storage and further evaluation. Samples were observed with a CCD camera at a resolution of about 20 μm.

The instrument is equipped with a number of different IR-lasers. An OPO laser system (Mirage 3000B, Continuum, Santa Clara, CA) pumped by the fundamental and second harmonic of a Nd:YAG laser (Surelite II-10, Continuum) served as wavelength-tunable laser source. Wavelengths between 2.12 and 4.0 μm have been employed in our study. The width of the OPO laser pulse is 6 ns (FHWM). Two solid-state erbium lasers were employed as fixed-frequency lasers emitting at 2.79 μm (Er:YSGG) and 2.94 μm (Er:YAG). The Er:YSGG laser was an SEO 1-2-3 (Schwartz Electro Optics, Orlando, FL; pulse duration, 70 ns, Q-switch mode). The Er:YAG laser (Speser, Spektrum Laser GmbH, Berlin, Germany) was also used in Q-switch mode. The pulse duration of this laser can be adjusted to some extent between ca. 70 and 200 ns by variation of the delay between flash tube discharge and electro-optical switching. A laser pulse duration in between 90 and 100 ns was used in the described studies. All three lasers were emitting with Gaussian-shaped temporal pulse profiles, as measured with a fast IR-sensitive HgCdTe-detector (Radec Infrared-Detector R004-0, Boston Electronics Co., Brooklin, MA; time resolution $\lesssim$5 ns).

Three transversely excited atmospheric pressure (TEA) CO_2-lasers (all from Laser Science, Inc., Franklin, MA) with emission lines of 9.25, 9.59, and 10.59 μm were used for IR-MALDI in the 10 μm wavelength range. The widths of the principal first spike of these lasers were 110, 130, and 80 ns, respectively, followed by a slowly decaying tailing of low intensity for up to 1.5 μs.

In the also reported earlier experiments by Ehring (chapter 3.2.2), a different CO_2 laser ($\lambda = 10.6$ μm; Excimer laser 500, Lumonics, Ottawa, Canada) was used. The output of this laser consisted of a principal pulse of ca. 100 ns in length, followed by a tailing of lower intensity on the order of several hundred nanoseconds. In the study by Ehring, the Er:YAG and Er:YSGG lasers also emitted with somewhat longer than the above pulse durations (ca. 150–200 ns) due to the use of different optical switches.

All IR-laser beams were coupled into the mass spectrometer via the same port and hit the sample at an angle of incidence of 45°. CaF_2 lenses and vacuum windows were used in the 3 μm wavelength range and ZnSe substrates for the CO_2-laser lines. The instrument was also equipped with a standard N_2-laser for UV-MALDI (VSL-337ND, Laser Science, Inc., Franklin, MA; $\lambda = 337$ nm, $\tau = 3$ ns). The $1/e^2$-focal spot sizes of all lasers were in the range of 100–300 μm in diameter. Identical foci were

used in the comparison experiments in which possible laser wavelength and pulse duration effects were investigated.

2.2. Photoacoustic experiments

The photoacoustic detector was constructed in-house on the basis of a sensitive piezoceramic transducer (FPM202, Marco, Dachau, Germany). This sensor had a thickness of 5 mm, a diameter of 10 mm, and was metallized on both sides with a thin layer of CuNi for electrical contact. The detector disk was mounted high voltage (HV)-proof into a modified MALDI target. Signals were coupled out via HV condensators, amplified by a fast differential amplifier, and fed into the second channel of the digital oscilloscope. The set-up allowed the parallel recording of mass spectrometric ion signals, which were recorded with the first channel of the oscilloscope. Only glycerol was investigated systematically as IR-MALDI matrix. Samples were prepared either directly on the transducer or on a PMMA spacer between sample and sensor in order to separate photoacoustic signal and electronic noise produced by the Nd:YAG pump laser of the OPO, picked up by the electrical circuit. Substance P was used as analyte and prepared in analyte-to-matrix ratios of $\sim 10^{-4}$. The transit time of stress waves through the detector disk was about 1.2 μs, sufficiently long to separate front and backside generated signals.

2.3. Sample preparation

All chemicals were purchased from Sigma Chemical Co. (Deisenhoven, Germany) or Fluka Chemical (Buchs, Switzerland) and used without further purification. Solid state matrices were prepared as standard dried-droplet preparations with typical analyte-to-matrix ratios of about 10^{-4}. Typically, H_2O or H_2O/ethanol mixtures were used as solvent for both matrix and analyte. Glycerol samples were prepared on-target by thoroughly mixing the neat matrix liquids with the aqueous analyte solution in a 1:1-volume ratio. Prior to insertion into the high-vacuum of the sample chamber, most of the water in the samples was gassed-off at a pressure of ca. 10^{-2} mbar in the transfer lock of the mass spectrometer.

3. Results and discussion

A number of work has been performed in the recent past to elucidate the different physico-chemical aspects of the IR-MALDI process. In the following, a concise overview over this work will be given, supplemented by, more comprehensively described, recent results from our laboratory. Reflecting the three initial stages of MALDI-TOF-MS, we have tried to arrange this chapter into three groups, desorption, ionization, and plume dynamics, although all three are of course intermingled to a certain extent. In the first two sections the role of the different laser and material (matrix) parameters in the desorption/ionization process is discussed and probable desorption/ionization mechanisms are addressed. The third section provides a description of recent measurements on the dynamic parameters (kinetic energies) of the expanding MALDI plume and a discussion of their influence on the performance of time-of-flight instruments.

3.1. Desorption

3.1.1. Influence of the laser wavelength

Most of the reported fundamental work addressed the role of the laser wavelength in the process, in particular for the range of the O–H, N–H, and C–H stretch vibrations of IR matrices (2.7–4.0 μm). Either wavelength-tunable OPO lasers [16,17–20] or the Vanderbilt FEL [21–24] were used in these studies. Making use of the tunability of the FEL over a wider wavelength range, Cramer et al. [21,22], Hess et al. [23], and Papantonakis et al. [24] extended the wavelength studies to the absorption by C=O stretch vibrations between 5.5 and 6.5 μm. Results for the 10 μm wavelength range, in which absorption occurs via the O–H bending and C–O stretch vibrations of suitable matrices, were obtained recently in our laboratory and are presented as part of this article.

It is helpful to differentiate between the three wavelength ranges:

3.1.1.1. 2.5–4.0 μm wavelength range. The most remarkable finding in this wavelength range is probably the surprisingly low threshold fluence for typical IR-MALDI matrices at wavelengths $\lesssim$3.0 μm, without corresponding bands in the IR-absorption or transmission spectra of the compounds. Compared to the low-light-intensity infrared spectra, either a blue-shift or a significant broadening of the threshold fluence vs. wavelength curves towards lower wavelengths were reported for a variety of matrices [16,18,19,21–23]. An example from a recent comprehensive investigation by the authors on a series of matrices with different chemical structure [16] is depicted in Fig. 1. This figure shows the wavelength-dependent threshold fluence for the generation of cytochrome *c* ions along with the IR-transmission spectrum of the used glycerol matrix. Compared to the IR spectrum, the threshold fluence curve of the O–H stretch band around 3 μm is "blue-shifted" by about 130 nm. For the longer wavelengths of the C–H stretch vibration modes around 3.4 μm, the spectral courses of the threshold fluences were, however, found to track essentially those of the IR-absorption for all matrices.

Together with some supplementary experiments on the mechanisms, as reported in [16], these results

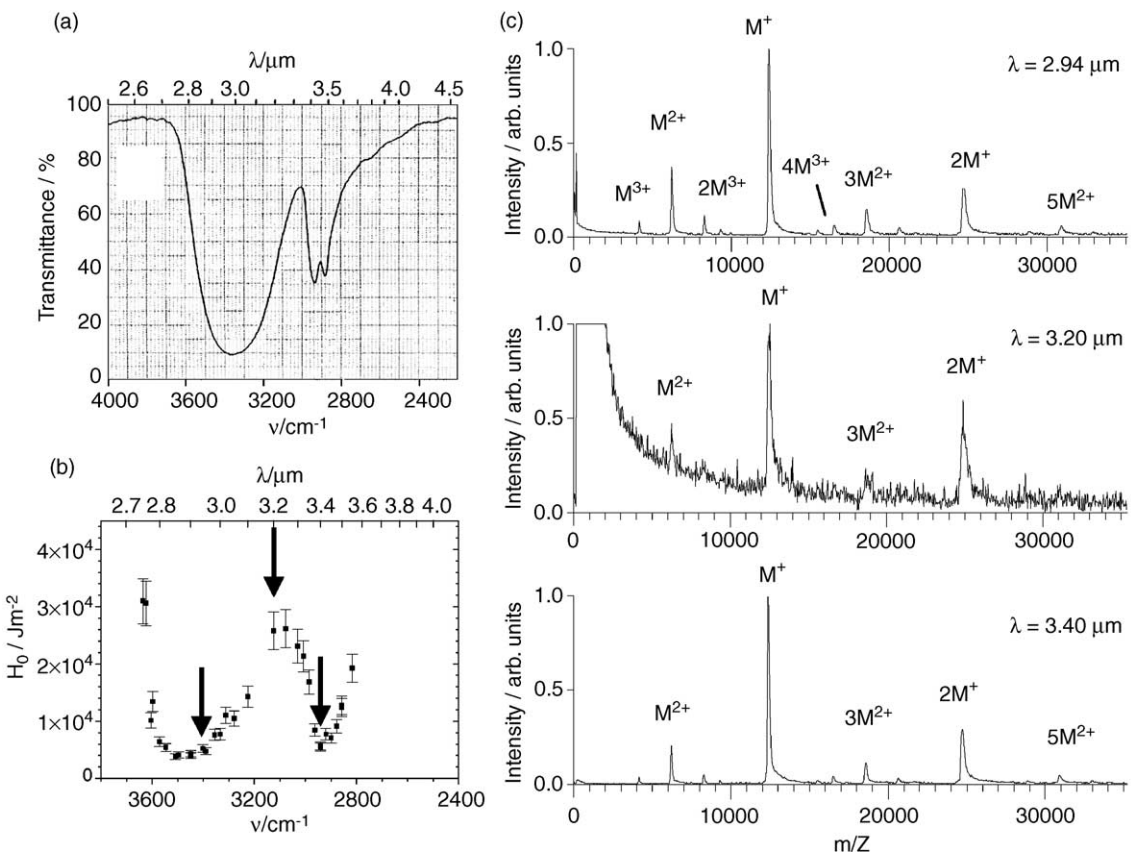

Fig. 1. (a) IR-transmittance of glycerol as a function of wave number ν and wavelength λ. (b) Wavelength-dependent threshold fluence $H_0(\lambda)$ for desorption of cytochrome *c* ions from glycerol. (c) Reflector TOF IR-MALDI mass spectra of cytochrome *c* ions desorbed from a glycerol matrix at different wavelengths λ of 2.94, 3.20, and 3.40 μm. The arrows in (b) indicate the laser excitation wavelengths.

suggested that modified absorption profiles by weakly hydrogen-bound OH and NH groups form the principal reason for the deviations around 3.0 μm. We assumed these effects to be caused by either transient laser heating of the matrices, resulting in a thermal or even acousto-mechanical weakening of intermolecular hydrogen bonds, and hence strengthening of the intramolecular binding with corresponding change in the absorption profile. In an alternative explanation, strong contributions from surface or interstitial molecules, lacking the intermolecular hydrogen binding of the functional groups, were also discussed as a potential reason for a broadened absorption profile. For the liquid matrix glycerol, a dynamic "bootstrap-like" generation of weakly bound absorbers during the laser pulse could indeed be monitored by laser transmission experiments on thin glycerol films [16].

Absorption by residual crystal water or water of hydration has previously also been discussed by several researchers as possible energy deposition pathways [19,20,22,25]. Clear experimental evidence for such an effect could, however, not be obtained so far [16].

Best mass spectrometric performance with respect to signal-to-noise ratio and achievable mass resolution has consistently been found in all studies at those wavelengths for which also low threshold fluences were determined. Fig. 1c shows this examplarily for a cytochrome *c*/glycerol system for three excitation wavelengths of 2.94, 3.20, and 3.40 μm.

3.1.1.2. 5.5–6.5 μm wavelength range. Investigations in this wavelength region of C=O stretch vibrations were carried out by Cramer et al. [21,22]. For this vibration mode, essentially conform spectral courses of absorption and threshold fluences were recorded. In two subsequent FEL studies by Hess et al. and Papantonakis et al., a small blue-shift for the C=O band was, however, reported for succinic acid [23,24]. In agreement with the 3 μm results the best mass spectrometric performance has generally been obtained at wavelengths of low threshold fluence.

3.1.1.3. 10 μm wavelength range. We have recently investigated the wavelength dependence of ion generation in this wavelength range of C–O stretch and carboxylic O–H bending vibrations to some detail, in extension of previous work on the feasibility of IR-MALDI with μ-TEA CO_2 lasers [7]. Three μ-TEA CO_2 lasers (all from Laser Science, Inc., Franklin, MA) with emission lines of 9.25, 9.59, and 10.59 μm were tested in this study. Experiments were performed with glycerol, lactic acid, and diethanolamine. Solid state matrices were not investigated because of a rather poor shot-to-shot reproducibility in this 10 μm wavelength range [7]. Also for the tested liquid matrices, the assessment of exact ion threshold fluence values turned out to be problematic with these CO_2 lasers, because of residual temporal pulse tailing and, compared to the 3 μm lasers, less well defined spatial beam profiles. Only the overall mass spectrometric performance was, therefore, evaluated in dependence of laser wavelength and matrix absorption characteristics.

The three investigated liquid matrices exhibit a strong modulation in their absorption profile around 10 μm. As an example, the IR-transmission spectrum of glycerol is shown in Fig. 2. For this compound, the highest absorption is found at 9.59 μm, followed by that at 9.25 μm. At the most common CO_2 laser wavelength of 10.59 μm, the absorption of glycerol is, however, rather weak. The differences in transmission between the three wavelengths, as taken from Fig. 2a, correspond to about 9 and 17 times higher absorptions at 9.25 and 9.59 μm than at 10.59 μm, respectively. In fact, the absorption coefficients at both 9 μm wavelengths are even comparable to those at the two pronounced O–H and C–H bands at 2.9 and 3.4 μm (Fig. 1a, [26]), respectively, for which excellent spectrum qualities are found (Fig. 1c).

The higher absorption at 9.25 and 9.59 μm is, however, not accompanied by advantageous desorption/ionization properties (Fig. 2b), in distinct contrast to the above results for the 3 μm wavelength range. In fact, the by far best mass spectra are obtained at 10.59 μm. Taking the different signal-to-noise ratios and the general shot-to-shot variability into account, the general ion patterns in the three mass spectra are furthermore likely rather similar than relevantly different, although for the concrete spectra of Fig. 2

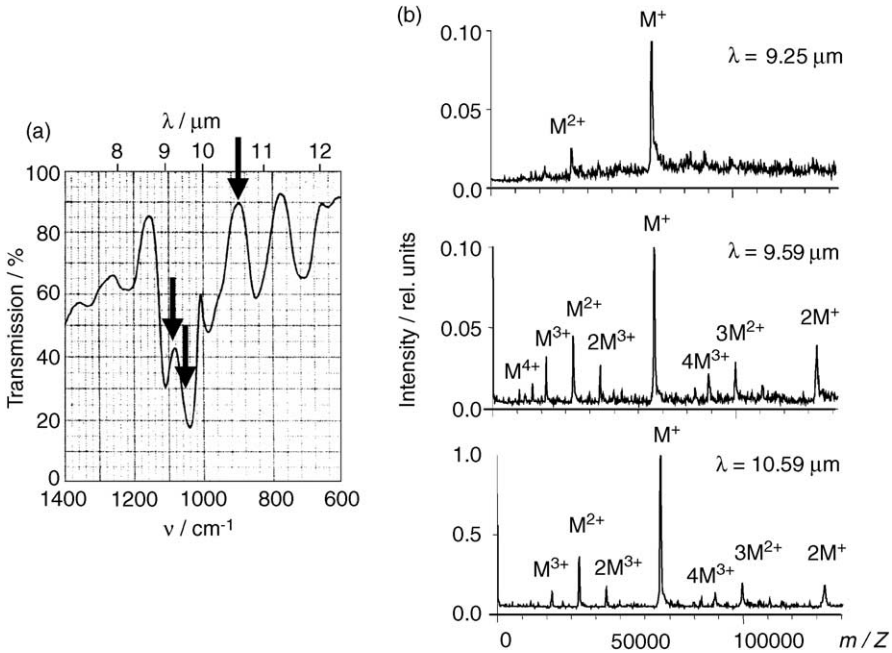

Fig. 2. (a) IR-transmittance of glycerol as a function of wave number ν and wavelength λ. (b) Reflector TOF mass spectra of bovine serum albumin (BSA) ions desorbed from a glycerol matrix at different wavelengths λ of 9.25, 9.59, and 10.59 μm. Note the different intensity scales of the mass spectra. The arrows in (a) indicate the laser excitation wavelengths.

a somewhat higher abundance of multiply charged BSA oligomers is notable for the 9.59 and 10.59 μm wavelength.

Desorption/ionization at 10.59 μm was visibly accompanied by explosive material ablation, a process which obviously supports the generation of charges. Control experiments with a non-absorbing ZnSe substrate proved that eventual energy deposition via the stainless steel target did not contribute notably to the overall process. The results are also in qualitative agreement with earlier unpublished work by Cramer, carried out during his time in our group. These latter experiments from the early phase of IR-MALDI were performed with a different TEA CO_2 laser with relatively poorly defined temporal pulse profiles and solely for solid state matrices.

It is actually difficult to understand why comparable energy densities in the 3 μm-bands and at 9.59 or 9.25 μm lead to largely dissimilar results. The more because also the rate of energy deposition, i.e., the laser pulse duration, is almost identical for both wavelength ranges. As the only obvious experimental difference, the primary energy deposition into C–O instead of O–H, (N–H) or C–H stretch vibration modes remains as a potential reason for the different extent of ion generation. More work is, however, clearly necessary to further elucidate the reasons for these interesting experimental findings.

3.1.2. Influence of the laser pulse duration

The laser pulse duration forms the second important irradiation parameter. We have recently investigated its role in the energy deposition in IR-MALDI for wavelengths of 2.79 and 2.94 μm [27]. In this work, two fixed-frequency Er-lasers with pulse durations τ of 75 ns (Er:YSGG, $\lambda = 2.79$ μm) and 90 ns (Er:YAG, $\lambda = 2.94$ μm) were compared to the OPO laser (tuned to either of the two erbium laser wavelengths) with its short pulse duration of 6 ns. A reduction in threshold fluence within a factor of 1.2–1.7 was observed

in this study for common IR-matrices by going from the 90 ns of the Er:YAG-laser to that of 6 ns of the OPO. For the Er:YSGG laser, this reduction was somewhat less pronounced but also noticeable. The notable tendency towards a lower threshold fluence for OPO laser excitation is likely to reflect photomechanical effects caused by partial stress confinement, as has been discussed by Zhigilei et al. [28,29]. In this molecular dynamic simulation work, threshold fluences were calculated to drop by the same order of magnitude for the transition from thermal (no energy transport by heat diffusion, but dissipation of photoacoustic stress) to stress confinement (no energy transport by thermal and photoacoustic pathways). The possible relevance of the photomechanical processes are discussed further in Chapter 3.1.5. of this article.

Mass spectra (i.e., analyte ion distributions, intensities and mass resolution) were not affected notably by the laser pulse duration for most of the tested matrices. Glycerol, the only liquid matrix tested in the investigation, however, formed an remarkable exception. With this matrix, enhanced multiple analyte protonation takes place when the 6 ns laser is employed and proteins are analyzed. Two representative glycerol-MALDI spectra of bovine serum albumin (BSA) are plotted in Fig. 3 to illustrate this pulse duration effect. Whereas abundant multiple protonation is observed with the OPO, as compared to the Er:YAG laser, the formation of unspecific oligomer ion complexes seems to be suppressed.

Abundant generation of multiply charged protein ions has also been reported before for some solid state matrices, for instance caffeic acid [4]. Our recent study revealed that for these matrices charge state distributions are, however, pulse duration independent in the probed range. The properties which distinguish the latter matrices are not known. In case of glycerol, they are likely to be caused by the different heating rates and time scales of the ablation process, as indicated by the photoacoustic study described in chapter 3.1.5. Both, a change in ionization efficiency, e.g., by enhanced re-neutralization of higher charge states in case of the 100 ns pulse [30], as well as either an enhanced decay of oligomers in case of the higher heating rate

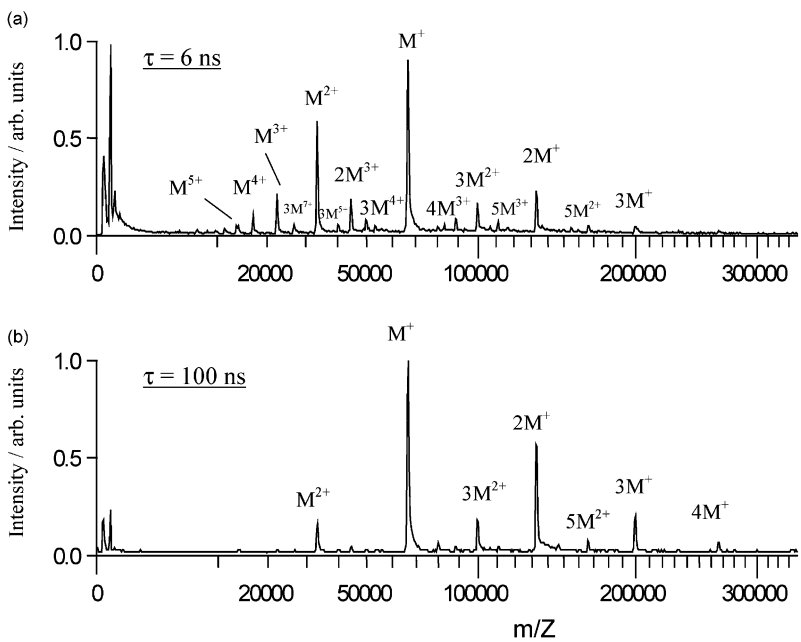

Fig. 3. Reflector TOF mass spectra of bovine serum albumin ions desorbed from a glycerol matrix, as a function of laser pulse duration τ: (a) $\tau = 6$ ns (OPO laser, $\lambda = 2.94\,\mu$m); (b) $\tau = 100$ ns (Er:YAG laser, $\lambda = 2.94\,\mu$m).

of the OPO laser, or a reduced generation of oligomers due to a possibly less dense plume, are conceivable to contribute to the experimental outcome.

Cramer et al. have previously also reported measurements on the effect of the laser pulse duration in IR-MALDI, performed in that work with the FEL laser. Macropulses in between ca. 100 ns and a few microseconds in duration were switched out by means of an electro-optical switch; an Er:YAG laser of 200 ns pulse duration was furthermore used for comparison [22]. For the pulse duration range and laser systems tested in this work, irradiance rather than fluence was found to be the determining irradiation parameter, in certain contrast to our study. The reasons for this discrepancy are not known, they are likely related to the very different pulse structure of the laser systems however.

3.1.3. Influence of the laser fluence and laser spot size on the ion signal intensities

The deposited laser energy per volume of material forms one of the most informative physical quantities for an assessment of the underlying desorption/ablation processes. Strikingly different energy densities at MALDI threshold fluences have been determined in a previous study by the authors for some common IR-matrices [31]. In this study, an Er:YAG laser was used. A fiber optic set-up ensured particularly well defined irradiation conditions (flat-top beam profile). For succinic acid with the lowest absorption of all tested matrices, energy densities as low as $2\,\mathrm{kJ\,mol^{-1}}$ were determined for volume elements close to the sample surface. Such a low energy density at MALDI threshold has been recognized before for this matrix [22,54] and has triggered speculations about spallation as the predominant solid state disintegration mechanism. 2,5-Dihydroxbenzoic acid (DHB) and thiourea have a larger absorption coefficient than succinic acid at 2.94 μm by a factor of 2.5–5 (DHB) and 20–45 (thiourea), but nevertheless exhibit essentially identical MALDI threshold fluences of about $1000\,\mathrm{J\,m^{-2}}$ [31].

Although glycerol exhibits the highest absorption coefficient of the tested matrix compounds of $100–200\,\mathrm{l\,mol^{-1}\,cm^{-1}}$ at 2.94 μm, higher MALDI threshold fluences by about a factor of two to three were determined for this matrix. Volume energy densities on the order of $50–100\,\mathrm{kJ\,mol^{-1}}$ or 0.5–1 eV per molecule are, hence, calculated for surface volume elements. These values are close to both, typical values for UV-MALDI [32], and the enthalpy of vaporization of $75\,\mathrm{kJ\,mol^{-1}}$ of this compound. The surprisingly different volume energy densities clearly indicate considerably different desorption/ionization mechanisms for solid and liquid state matrices.

The influence of the laser fluence on the analyte ion signal intensities was also investigated in the latter study. For all matrices, a strong increase of analyte ion intensity with laser fluence was determined. Fig. 4 displays this increase for angiotensin I ions, desorbed from the four investigated matrix compounds, glycerol, succinic acid, thiourea, and 2,5-DHB.

Finally, also the effect of the laser spot size (size of irradiated area) on the ion signal intensities was investigated in the said study [31]. For all matrices, a decrease of irradiation area was found to be accompanied by a strong increase in threshold fluence.

A general problem in the interpretation of the data obtained in the so far described work is given by the fact that all of these investigations relied solely on the recording of the mass spectrometric ions. The convolution of desorption and ionization mechanisms makes assessments about either of the two processes, however, inherently difficult, and the product ion data may even conceal relevant features of the two intermingled processes. Several of the above observations, like, e.g., the largely dissimilar deposited energies per volume for the different matrices and the discrepancies between wavelength courses of threshold fluences and molar absorption, may in fact indicate that a second (possibly strong) and so far more or less unknown wavelength dependence for the ionization step exists.

3.1.4. Photoacoustic study of material ablation (preliminary results)

In order to deconvolute both processes to some extent and to extend the previous work to the analysis of overall material ablation, a photoacoustic experiment

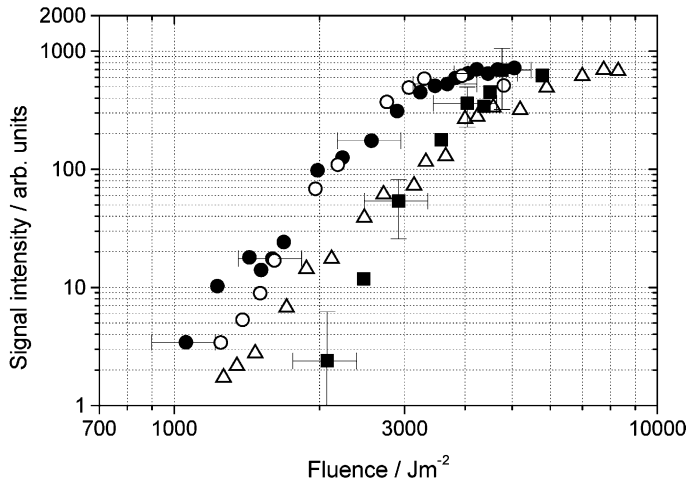

Fig. 4. Signal intensities of angiotensin I ions as a function of laser fluence and for desorption from different matrices: (●) DHBs; (○) thiourea; (△) succinic acid; (■) glycerol. An Er:YAG laser ($\lambda = 2.94\,\mu m$, $\tau = 90\,ns$), coupled into a fiber optical set-up to produce a defined laser spot diameter of 350 μm on the sample, was used for desorption/ionization. Reproduced with permission from [31] (copyright 2000, © John Wiley & Sons Ltd.).

was recently set up in our laboratory. Pressure waves generated by the interaction of the laser light with the sample were detected with a sensitive piezoceramic transducer on which the samples were prepared. Only glycerol has been investigated systematically in these experiments so far.

Typical photoacoustic signals as generated by the OPO, tuned to the Er:YAG laser wavelength of 2.94 μm (pulse duration, 6 ns), and the Er:YAG laser (pulse duration, ∼100 ns) are presented in Fig. 5 for low, i.e., "sub-ablative" laser fluence, a fluence slightly above MALDI ion threshold, and for an elevated laser pulse energy. At low fluences (Fig. 5a), photoacoustic signals are generally bipolar and symmetric. The compressive first component is simply the result of thermal heating and expansion of excited volume elements. The second tensile component of the signal results from the reflection of the compressive stress wave at the surface–vacuum interface. Because material expansion is fully reversible at these low fluences, this symmetric bipolar signal is commonly characterized as thermoelastic. In agreement with photoacoustic theory, we found the amplitude of thermoelastic signals to rise exactly linearly with fluence. Shape and width of the thermoelastic signal produced by the Er:YAG laser were also found to agree with the solution of hydrodynamic stress wave equations, calculated according to [33] and extended in our study for the given sample and irradiation conditions. In the case of the OPO laser, thermoelastic signals are, however, wider than predicted by the simple theory by about a factor of two to three, for not yet fully known reasons (possible causes are the opening angle of the spherical stress wave, resulting in an arrival time distribution at the planar detector surface, and dispersion).

At higher fluences, thermoelastic signals are superimposed by a second, purely compressive component, which can be directly related to the recoil momentum of ablated material (Fig. 5b and c). Because of the linearity of the thermoelastic signal, the ablation-induced compressive component can be straightforwardly extracted from the composite photoacoustic signal by extrapolation. The results of this deconvolution are shown in Fig. 5c for the OPO and Er:YAG laser respectively. Whereas, in the first case, ablation is confined to ∼30 ns, considerably prolonged material ablation with an approximately exponential decay characteristic (time constant, ∼1 μs) is recorded for the Er:YAG laser, reminding of a vaporization-like process.

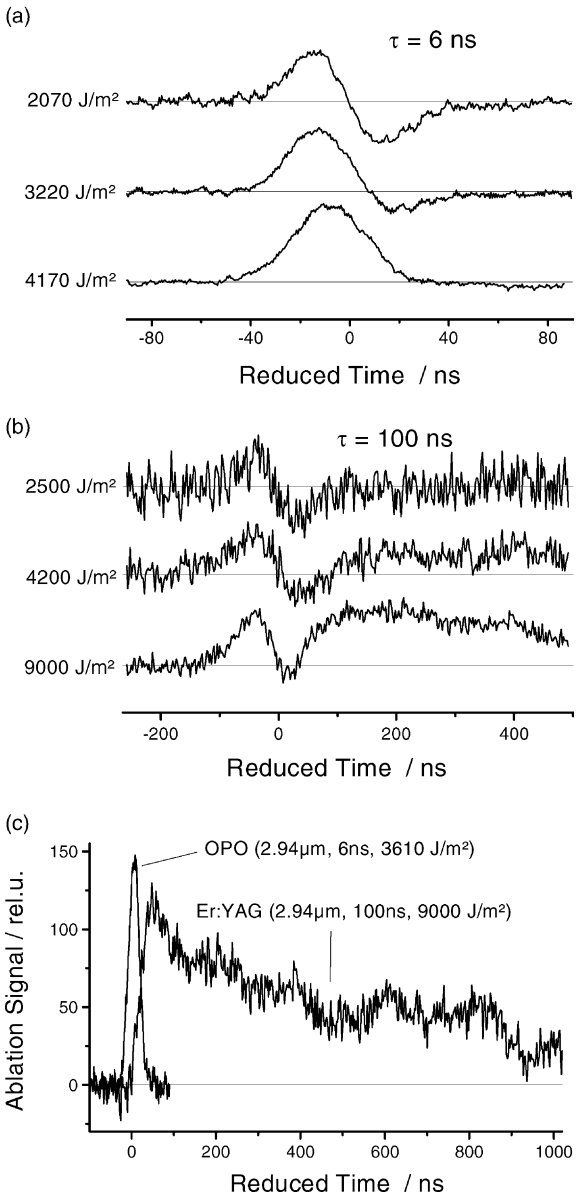

Fig. 5. Photoacoustic stress waves generated by (a) OPO and (b) Er:YAG laser excitation in glycerol at a wavelength of 2.94 μm and recorded by the piezoelectric transducer after passage through the glycerol drop. Displayed are photoacoustic signals generated at fluences below and slightly above MALDI ion threshold (upper two traces), and at an elevated fluence (bottom trace). The two traces in (c) represent the deconvoluted ablation signals, proportional to the ablation rate (see text for further explanation). "Reduced time" denotes the "arrival time" of stress waves at the detector minus the propagation time of the acoustic signal through the sample.

The study also revealed that with both lasers notable vaporization of glycerol sets in already considerably below the MALDI ion threshold fluence [34]. The increase of the ablation-related signals with fluence was, moreover, found to be weaker than that of the corresponding ion signals. The details and results of these experiments will be described comprehensively in a separate publication.

The temporal profiles of the ablation signals point to considerably different ablation mechanisms for excitation with the two laser pulses. These differences can be rationalized if laser excitation and stress relaxation times are compared; thermal confinement conditions are fulfilled for both lasers. For the given large aspect ratio (laser spot size, ∼150 μm; laser penetration depth δ, ∼1.5 μm at 2.94 μm), the photoacoustic relaxation time τ_s is usually defined by the transit time of stress waves through the excitation volume, i.e., $\tau_s = \delta/v_s$, where v_s is the velocity of sound in the material. With v_s ∼2000 ms^{-1} and δ ∼1.5 μm for glycerol [16], τ_s follows to ∼0.8 ns. Taking into account the reflection at the surface–vacuum interface, τ_s will in reality be somewhat higher and on the order of 1–2 ns. Although still lower than the laser pulse duration of 6 ns, build-up of stress is likely to be relevant in this case. For the Er:YAG laser photoacoustic stress will, on the other hand, dissipate essentially within the laser pulse duration of ∼100 ns.

The results from the photoacoustic study can also be compared to recent molecular dynamic (MD) simulations by Zhigilei and coworkers [28,29], revealing comparable temporal profiles of stress waves for experiment and simulation. A limitation of the MD method is, however, formed by the comparably low maximum simulation volume of 100 nm in depth, one to two orders of magnitude below the experimental IR-MALDI conditions. Further details of the MD approach and comparison with experimental results are discussed in the article of Zhigilei et al. in this issue [29].

3.1.5. Models for the desorption/ablation process

Summarizing the so far described work, a rather complex picture evolves for the MALDI desorption

process with pulsed infrared lasers. The actual pathways via which material ablation proceeds appear to depend on the concrete properties of the matrix and the laser irradiation parameters, rather excluding a "universal" desorption model. In particular, one apparently has to differentiate between desorption from solid and that from liquid state matrices. Quite different models have, in fact, also been put forward in the literature, ranging from spallation, as an effective low energy density process [22,35], over photoablation in different effective forms [28] to basically thermal models [31]. A large body of information can moreover be extracted from related studies on laser–material interaction, e.g., from those on laser ablation of hard and soft biological tissue or of technical material processing [36,37].

According to the original work by Dingus and Scammon [35], front surface spallation will occur if the tensile component of the laser-induced stress wave exceeds the material strength. As discussed above, stress confinement conditions are indeed fulfilled for certain IR-matrix/laser combinations, e.g., for the combination of succinic acid, 2.94 μm laser wavelength and the 6 ns OPO pulse duration. For the 100 ns pulse duration of the Er:YAG laser, stress confinement conditions are still partly fulfilled. Spallation has consequently been assumed by some authors to be a dominant mechanism in IR-MALDI [22,54]. Our experiments on the laser pulse duration effect, however, rather disprove these consideration because in contrast to the spallation model, even for the weakly absorbing matrices like succinic acid only a rather low change in threshold fluence was found upon change of the laser pulse duration in the critical range.

Taking glycerol as the other extreme with a high energy density per volume, basically thermal processes appear to form the relevant if not predominant mechanisms. In fact, the energy densities in excited glycerol on the order of 100 kJ mol^{-1} [31] are very similar to those in UV-MALDI [31]. In contrast to excitation in the UV, laser penetration depths are higher by one order of magnitude, however, for glycerol and on the order of one to a few micrometer, depending on the laser wavelength. Provided a fast-enough heating rate, superheating of the material is, therefore, likely to occur and to lead to both bubble formation in the overheated sub-surface layers and possibly to phase explosion [28].

Considerably more work than on glycerol has naturally been performed on laser ablation and laser-induced cavitation effects of/in water or water-containing tissue [36,38–43]. Water exhibits not only a comparably high absorption at around 3 μm as glycerol but also comparable other relevant physicochemical properties. A comparison of these results with those of glycerol-IR-MALDI appears therefore very meaningful. For water, quite diverse processes, depending on wavelength (absorption), laser fluence and pulse duration, have, in fact, been determined in these investigations [42]. For water, (micro-)cavitation (bubble) formation, induced either directly by laser heating and/or supported by the photomechanical tensile stress, have indeed been found to form a dominant mechanism for rapid laser-induced disrupture and conditions comparable to those for IR-MALDI [44,45]. Recent molecular dynamics simulations by Zhigilei and Garrison in which the formation of voids has been observed for stress confinement conditions further support these considerations for the IR-MALDI case [28]. The disrupture or possible collapse of such micro-bubbles/voids is moreover forming rather energetic processes. Such mechanisms are, therefore, also likely to contribute to primary charge generation.

3.2. Ionization

3.2.1. Primary charge generation and secondary ion–molecule reactions

The actual pathways which lead to analyte ionization in IR-MALDI must be regarded as hitherto only poorly understood. This assessment seems particularly true for the primary ion generation, whereas thermodynamically controlled secondary ion–molecule reactions in the plume involving a high number of collisions in a dense environment are believed to lead to an efficient ionization of analytes, once a sufficient concentration of primary ions or electrons is available

[46–50]. Probable secondary ion–molecule reactions have been discussed in detail recently by Knochenmuss et al. [48]. Although particular emphasis was put in this work on the UV-MALDI case, similar if not identical secondary mechanisms should be expected to occur in the IR-MALDI plume.

With respect to the preceding step, the primary charge generation, it has been suggested by different authors that the rapid break-up of material by cavitation, explosive phase transition, or spallation could form sufficiently energetic processes. In case of IR-MALDI from liquid matrices, processes similar to "spray ionization" (aero- or thermospray ionization [51]) are likely to form additional possible pathways for analyte ionization, although more work clearly has to be carried out to further elucidate this aspect. Quite remarkable in this context are recent results by Iavarone et al. who showed that the addition of glycerol to acidified electrospray ionization (ESI) solvents can strongly enhance multiple protonation of analytes in ESI-MS [52]. In particular ion formation in IR-MALDI with glycerol can, moreover, also be directly compared with previous studies on ion formation from glycerol in liquid secondary ion mass spectrometry/FAB [46,53] (see below). The observed strongly dissimilar ionization efficiencies in the 3 and 10 μm wavelength ranges (chapter 3.1.1.) will moreover have to be taken into account for a comprehensive picture for this matrix compound.

3.2.2. Generation of quasimolecular matrix ions as a function of laser wavelength

A rather complex picture of ion formation is also indicated if the above wavelength studies are extended to a thorough analysis of the wavelength dependence of matrix ion generation. Although such an analysis appears to be one of the most straightforward, even almost trivial approaches in the context of investigations on ionization mechanisms, it has hardly been addressed in the literature. As shown in this chapter, some interesting features can, indeed, be revealed from a detailed analysis of the mass spectra in the matrix ion mass range.

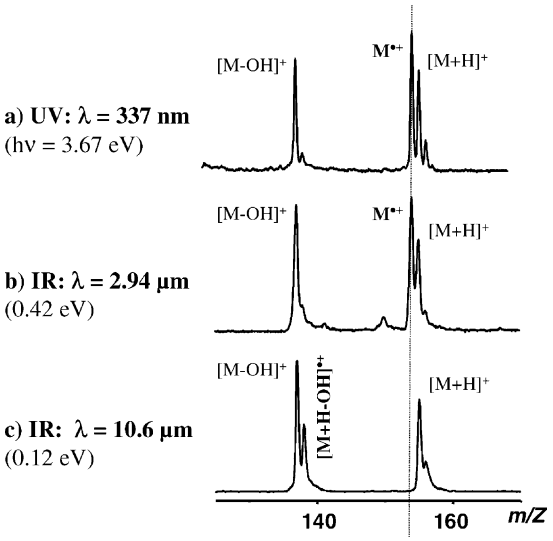

Fig. 6. Reflector TOF mass spectra of 2,5-DHB as a function of laser wavelength λ: (a) λ = 337 nm (UV-MALDI); (b) λ = 2.94 μm (IR-MALDI); (c) λ = 10.59 μm (IR-MALDI). Shown is the mass range of the quasimolecular ions.

As an example, three mass spectra of 2,5-DHB recorded at laser wavelengths of 337 nm, 2.94, and 10.59 μm, respectively, are displayed in Fig. 6. 2,5-DHB can, as most of the common UV-matrices, be used in all three wavelength ranges. Especially 2,5-DHB has, moreover, been recognized before as a practical test compound in comparative UV-IR studies [54].

The figure shows that despite the different (electronic vs. vibrational) excitation pathways identical DHB matrix mass spectra are obtained at laser wavelengths of 337 nm and 2.94 μm, with about equal relative abundance for the radical and protonated quasimolecular matrix ions at 154 and 155 Da. At 10.59 μm, the radical cation is, however, either not generated or is completely depleted in the course of the overall process. Instead, a somewhat increased abundance of $[M + H - OH]^{\bullet +}$ ions is now observed.

On first sight, the observation of abundant radical matrix ions in IR-MALDI appears surprising since the "direct" generation of the radical matrix cation, e.g., by photoionization or even by excited S_1 state proton transfer, can be ruled out for the rather low MALDI

Table 1
Observed quasimolecular ions of selected matrices as a function of excitation laser wavelength (adopted from [55])[a]

Matrix	UV-MALDI ($\lambda = 337$ nm)	IR-MALDI	
		$\lambda = 2.79/2.94\,\mu$m[b]	$\lambda = 10.59\,\mu$m
2,5-DHB	$M^{\bullet+}$, $[M + H]^+$, $[M - OH]^+$	$M^{\bullet+}$, $[M + H]^+$, $[M - OH]^+$	$[M + H]^+$, $[M - OH]^+$, $[M + H - OH]^{\bullet+}$
2,5-DHB, negative ions	$[M - H]^-$, $[M - 2H]^{\bullet-}$	$[M - H]^-$	n.m.
2,4-DHB	$M^{\bullet+}$, $[M + H]^+$, $[M - OH]^+$	$[M + H]^+$, $[M - OH]^+$	$[M + H]^+$, $[M - OH]^+$
Succinic acid	–	$[M + H]^+$, $[M - OH]^+$, $[2M + H]^+$, higher mass products	$[M + H]^+$, $[M - OH]^+$, $[2M + H]^+$, higher mass products
Sinapinic acid	$M^{\bullet+}$, $[M + H]^+$, $[M - OH]^+$	$M^{\bullet+}$, $[M - OH]^+$	n.m.
Caffeic acid	$M^{\bullet+}$, $[M + H]^+$, $[M - OH]^+$	$M^{\bullet+}$, $[M - OH]^+$	$M^{\bullet+}$, $[M - OH]^+$

n.m.: not measured; (–): non-absorbing at this wavelength.
[a] Cationized quasimolecular molecules, abundantly seen for some of the matrices, are not included here.
[b] In part of the study, 150–200 ns long pulses (instead of 70–90 ns) of the Er:YAG and Er:YSGG lasers were used, due to the employment of different optical switches.

photon fluxes and the low photon energies of 0.4 eV at 2.94 μm, and definitely at 10.59 μm where the photon energy is as low as 0.1 eV. These radical cations must therefore be attributed either to secondary (plume) reactions or to "direct" ionization mechanisms by the aforementioned rapid disintegration or phase transition of the condensed phase.

Table 1, adopted from the PhD thesis of Ehring [55], shows the wavelength dependencies of ion formation for selected matrices in the three wavelength ranges and confirms the complexity of ion generation mechanisms. A different CO_2 laser (Excimer 500 with modified IR-optics; Lumonics, Ottawa, Canada) with a pulse duration of ∼100 ns was used as described previously [5]. The laser emitted at a wavelength of 10.59 μm. Spectra were generated from neat matrix samples under continuous ion extraction conditions.

Besides the above discussed 2,5-DHB, the outcome for caffeic acid and sinapinic acid seems especially noteworthy. For these two matrices only the radical molecular ion is observed for IR excitation. The protonated quasimolecular ion, albeit detected in the UV next to the cation, is not present in the IR-MALDI mass spectra. Abundant $[M - OH]^+$ ions are, however, recorded. Ehring also noted a general increase of the ratio between radical and protonated ion intensities with IR-laser fluence, dissimilar to the UV. IR-spectra were, moreover, found to show a considerable variation in the ion signal patterns from shot-to-shot.

It is particularly important to point out, that, if only the analyte ion mass range were looked at, mass spectra would mostly look very similar for UV- and IR-MALDI as well as for the two IR-MALDI cases [6,7,56–58]. Such findings have previously led other researchers to conclude that very similar, if not equal desorption/ionization mechanisms, must be involved in UV- and IR-MALDI [56]. In view of the above results, this conclusion appears too simplified, however.

We have recently extended the work of Ehring to a detailed analysis of glycerol and excitation with the Er:YAG laser ($\tau = 90$ ns). The matrix ion regions from two representative, positive and negative ion mode mass spectra are plotted in Fig. 7. Again, a relatively high variation in ion signal pattern and signal intensities is found from exposure to exposure in the matrix ion region, whereas analyte ion intensities typically show exceptionally low scatter for desorption from glycerol. Alkali-cationized glycerol molecular signals form the base peak in the positive ion mode mass spectra (Fig. 7a). In the negative ion mode (Fig. 7b), adduct

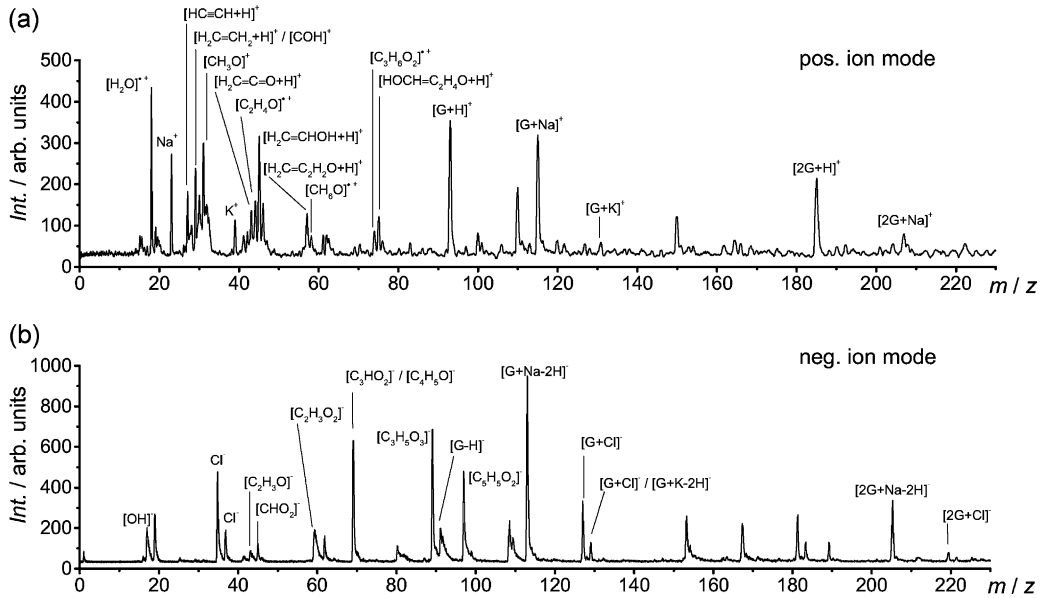

Fig. 7. Reflector TOF mass spectra of glycerol (matrix ion region) generated with the Er:YAG laser. (a) Positive ion mode; (b) negative ion mode. Some fragment ion signals have been assigned with their putative structure.

ions with Cl^-, singly deprotonated glycerol molecules or ions of the type $[G + \text{alkali} - H_2]^-$ form the most intense quasimolecular signals. The abundance of the alkali- and chlorine-related signals can be reduced to a certain extent by treatment of samples by ion exchange beads; as has been done in the sample preparation for Fig. 7. Analyte ion intensities were not notably affected by the purification. Glycerol oligomers of both protonated and alkali-cationized type are detected up to the 4-mer (not shown). A large number of product and fragment ions are furthermore present. The putative structures of some of the glycerol fragment ions are indicated in the figure. Next to various radical glycerol fragments of minor intensity, radical water ions, $H_2O^{\bullet+}$, are furthermore detected with high abundance. Together, the large number of different product and fragment ions points to an overall high reactivity of the MALDI plume. Very similar glycerol ion signal patterns have been identified before in a detailed study by Caldwell and Gross on fast atom bombardment (FAB) [53]. In this work detailed considerations about possible ionization mechanisms have also been made.

3.3. Plume dynamics

3.3.1. Kinetic energies of analyte and matrix ions

The achievable mass resolution and mass accuracy of an axial time-of-flight mass spectrometer is intrinsically affected by the dynamic properties of the generated MALDI plume, in particular by the width of ion velocity distributions. A good knowledge about these properties is therefore not only meaningful for a better basic understanding of the processes underlying MALDI but also for instrumental improvements. It is generally helpful to differentiate between the mean initial velocities of molecules or ions, on the one side, and their velocity and angular distributions, on the other.

We have recently investigated the mean axial initial velocities of a variety of matrix and analyte compounds, as well as the influence of the different irradiation parameters on these quantities [59]. This study revealed quite high mean initial velocities of IR-MALDI generated ions on the order of 700–1300 ms^{-1}, very similar to values for UV-MALDI. The initial velocities of analyte ions were found to be essentially determined

by the matrix from which they were co-desorbed and to approach those of the matrix ions. Consequently, mean analyte velocities are essentially independent of the molecular weight, which in turn leads to considerably high mean initial kinetic energies on the order of several 10 or even hundred electron volts for large compounds. Deviating results with lower analyte than matrix velocities have recently been reported by Ermer et al. [60]. This work focused on DHB as matrix and angiotensin II as analyte. The Vanderbilt FEL laser was used for desorption. The width of the velocity distribution was determined by Ermer et al. to be on the same order as the mean velocities, i.e., about 1000 ms^{-1} for the matrix and ~600 ms^{-1} for the analyte. Unpublished work by the authors confirmed this latter finding for various tested common matrix compounds [61,62]. Both widths of the distributions [61] as well as the mean initial axial kinetic energies [59] were found to be particularly large for liquid matrices. The measurements in [59] have furthermore indicated that analyte ions acquire a particularly large energy deficit upon desorption from liquid matrices and subsequent acceleration in axial TOF-instruments.

These differences in the plume dynamics for solid state and liquid matrices correspond directly to different mass spectrometric performances in combination with axial IR-MALDI TOF-MS instruments, and are particularly obvious if delayed extraction (DE) is applied. Whereas signal widths of analyte ions desorbed from solid state matrices generally correspond to those known from UV-MALDI (with a FWHM resolution on the order of 10,000 for the peptide mass range [7,10,63]), mass resolution is significantly lower by a factor of ca. two to three for IR-MALDI with glycerol as matrix [7,61].

Ion extraction conditions are, furthermore, a quite critical parameter if glycerol or other liquids matrices are employed. Generally, the application of low electrical field strengths in the first stage of ion extraction is favorable for these matrices, which is contradictory to optimal DE-conditions. The significant effect the electrical field strength has on the mass spectra is examplarily demonstrated in Fig. 8 for cytochrome *c* as analyte (MW, 12.360 kDa). Whereas low electrical

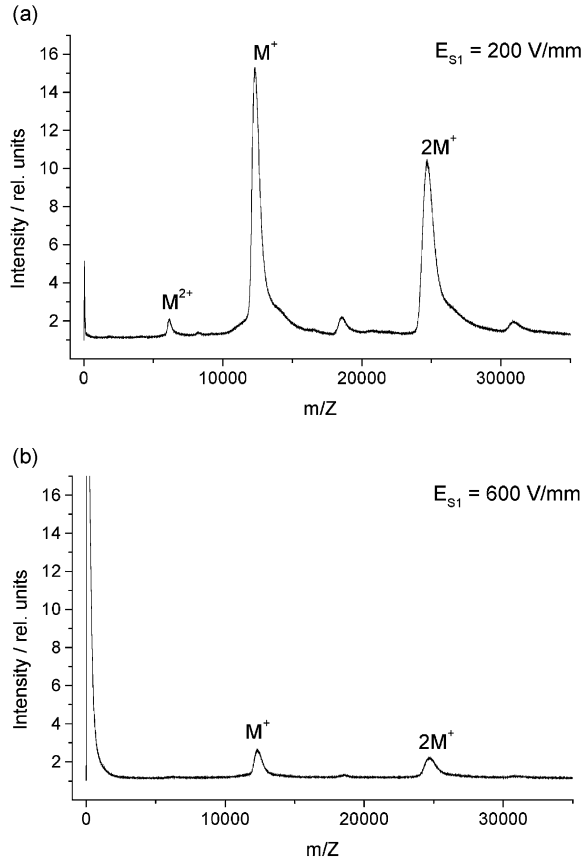

Fig. 8. Reflector TOF mass spectra of cytochrome *c* (MW, 12.360 kDa) desorbed from glycerol with the Er:YAG laser and obtained under different continuous ion extraction conditions (electrical field strength in the first extraction region, S_1, of the ion source; $S_1 = 6$ mm): (a) $E = 200\ V\ mm^{-1}$, (b) $E = 600\ V\ mm^{-1}$.

field conditions on the order of 200 $V\ mm^{-1}$ result in intense cytochrome *c* ion signals (Fig. 8a), increase of the electrical field strength gradually gives rise to high background ion intensities at low to intermediate *m/z*, and simultaneously to a decrease in protein signal, until the latter eventually disappears completely for yet usual instrumental field conditions. Fig. 8b shows the case of ~600 $V\ mm^{-1}$, as a typical value for (UV-MALDI) ion sources. Continuous ion extraction was applied in both cases. Full acceleration to the final kinetic energy of 16 keV is achieved in the second stage of the ion source, S_2, after thinning-out of the plume.

We found even lower electrical field strengths on the order of 100 V mm^{-1} to be advantageous, or even form a prerequisite in the analysis of very high molecular weight compounds, e.g., of large proteins and oligonucleotides [9]. This requirement has apparently been overlooked in some of the work by other groups and can explain occasional reports of rather disappointing results with glycerol.

Fig. 8 suggests that rather massive glycerol vaporization takes place under MALDI fluence conditions. The noted energy deficits [59] can therefore be explained by both, excessive collisions of ions in the plume upon extraction and a potentially strong field shielding effect by the dense material cloud. In fact, long delay times on the order of a microsecond (as compared to at most a few hundred nanoseconds, optimal for UV-MALDI and also IR-MALDI from solid state matrices) are advantageously used for desorption of peptides from the glycerol matrix [7]. All attempts to further improve the performance by using very long delay times with accordingly lowered extraction voltages in the two-stage ion source did not result in significant improvements with the current instrument, possibly simply because of the strong trade-off caused by the spread in space and time due to the then very long initial plume propagation times. The maximum adjustable length, S_1, of the first acceleration stage of the instrument, was 8 mm.

The latter assumptions are also supported by recent results by Cramer and Burlingame. These authors introduced a special target design in which liquid matrix samples are prepared in a vial in order to allow for a very defined field-free expansion prior to ion extraction [64]. In fact, this approach resulted in the standard high mass resolution of the used instrument for the peptide mass range. Some obvious drawbacks in terms of the analytical usefulness of this approach are, however, formed by the more complicated sample preparation, higher requirements on laser positioning, and a considerably limited view on the samples.

Concluding from the above results and the described instrumental achievements by Cramer and Burlingame, two aspects appear particularly important to accomplish for a better use of liquid IR-MALDI matrices and improvement of mass resolution. The first would, in analogy to the approach by Cramer and Burlingame, be a “thinning-out” of the dense initial plume prior to ion extraction, in order to minimize collisions of analyte ions with other plume constituents and field shielding effects. Second, a “thermalization” of particle (ion) velocities, i.e., generation of kinetic energy distributions with a small width, appears to be highly desirable. At present it seems at least doubtful, however, whether these requirements can be satisfyingly met with the current ion source designs on axial-TOF instruments.

3.3.2. Coupling of IR-MALDI with other than axial-TOF analyzers

A promising approach to overcome the described problems is the combination of IR-MALDI with analyzers for which the initial plume dynamics are less relevant. Three combinations of IR-MALDI sources with an orthogonal TOF (o-TOF), an FT-ICR instrument, and a quadrupole ion trap have indeed been introduced successfully, recently.

The combination of IR-MALDI with an o-TOF instrument was reported by Bromirski et al. [14,15]. An Er:YAG laser was employed in this joint work and peptides and oligonucleotides were desorbed from different common IR-matrices. Best results were reported for glycerol as matrix [14]. The essential aspect of the coupling is the thermalization of the glycerol/analyte plume in the first quadrupole of the instrument (filled with a suitable thermalization gas) and the thereby generated quasicontinuous ion beam with very low energy spread in the direction of final ion extraction. In other words, the initial dynamic properties of ions have been transformed after passage through the quadrupoles. A matrix and laser-independent mass resolution on the order of 10,000 (FWHM) was consequently achieved in the work by Bromirski et al. [14,15]. Whereas this study demonstrated that the advantageous features of glycerol-MALDI and a high mass resolution can be straightforwardly combined on this instrument, a yet to be solved problem is the occasionally extensive formation of analyte-glycerol adduct ions as a result of the thermalization.

To our knowledge, only the study by Budnik et al. has so far explored the combination of IR-MALDI with an FT-ICR analyzer [65]. A 4.7 T IonSpec instrument equipped with an Er:YAG laser of ~100 ns pulse width was employed in this work. Budnik et al. reported only results for solid state matrices, succinic acid and 2,5-DHB in this original work. Recent (unpublished) results obtained in cooperation with these authors showed that liquid matrices (glycerol) can also be used advantageously in this instrumental combination, and has, in fact, resulted in exceptionally high peptide ion intensities (data not shown).

The combination of an atmospheric pressure (AP) ion source with a quadrupole ion trap was, finally, described by Laiko et al., recently [66]. Desorption/ionization was here achieved by an OPO laser tuned to 3 μm. Laiko et al. demonstrated the detection of peptides in the mass range up to 2000 Da using glycerol and liquid water as matrices.

4. Conclusions

This article summarized the fundamental work on the mechanistics of IR-MALDI in the time period of about the last decade. Summarizing the findings from these investigations, it is evident that both, the advantageous properties of IR-MALDI, in particular its softness for the generation of ions from a wide class of (labile) analyte compounds, as well as current limitations in the mass spectrometric performance can be related to particular features of the desorption/ionization processes. The combined investigations revealed a rather complex picture of the IR-MALDI mechanisms. The concrete outcome of the laser–material interaction is generally strongly dependent on the actual laser and material parameters, for example the ratio between photomechanical relaxation times and laser pulse duration. The observation of a rather irregular wavelength dependence for the generation of quasimolecular matrix ions and that of abundant radical matrix ions for certain IR-MALDI matrices raised new questions about the affective ionization mechanisms. Preliminary results from a photoacoustic study revealed novel features, not visible in the ion data. This study pointed to a strong influence of the laser pulse duration for glycerol IR-MALDI.

Acknowledgements

The experiments reported within this publication were carried out in the laboratory of Prof. Franz Hillenkamp, to whom this issue of IJMS is dedicated on the occasion of his 65th birthday. The authors are grateful to him for the opportunity of exciting research and innumerable stimulating critical discussions.

A major part of the investigations on the quasimolecular matrix ion distribution as a function of desorption laser wavelength was performed by Hanno Ehring as part of his PhD thesis, carried out in the group in the years 1989–1993. Several others have contributed with their work to the development of IR-MALDI and to a better understanding of the underlying processes, and thereby influenced this article considerably. From these, Rainer Cramer, Michael Karas, and Andreas Overberg certainly had particularly large impact.

The μ-TEA CO_2 lasers were supplied by Laser Science, Inc., as part of a collaboration. Financial support by the Ministerium für Wissenschaft und Forschung (MWF) of the Federal state of Nordrhein-Westfalen under grant no. IVAI-800 985 96, the Deutsche Forschungsgemeinschaft (DFG) under grant no. HI285-8/2, and the Federal Ministerium für Bildung und Forschung (BMBF) under grant no. 0311419 is gratefully acknowledged.

References

[1] M.A. Posthumus, P.G. Kistemaker, H.L.C. Meuzelaar, M.C. Ten Noever de Brauw, Anal. Chem. 50 (1978) 985.
[2] M. Karas, D. Bachmann, U. Bahr, F. Hillenkamp, Int. J. Mass Spectrom. Ion Process. 78 (1987) 53.
[3] M. Karas, F. Hillenkamp, Anal. Chem. 69 (1988) 2299.
[4] A. Overberg, M. Karas, U. Bahr, R. Kaufmann, F. Hillenkamp, Rapid Commun. Mass Spectrom. 4 (1990) 293.
[5] A. Overberg, M. Karas, F. Hillenkamp, Rapid Commun. Mass Spectrom. 5 (1991) 128.

[6] S. Berkenkamp, C. Menzel, M. Karas, F. Hillenkamp, Rapid Commun. Mass Spectrom. 11 (1997) 1399.
[7] C. Menzel, S. Berkenkamp, F. Hillenkamp, Rapid Commun. Mass Spectrom. 13 (1999) 26.
[8] F. Kirpekar, S. Berkenkamp, F. Hillenkamp, Anal. Chem. 71 (1999) 2334.
[9] S. Berkenkamp, F. Kirpekar, F. Hillenkamp, Science 281 (1998) 260.
[10] R. Cramer, W.J. Richter, E. Stimson, A.L. Burlingame, Anal. Chem. 70 (1998) 4939.
[11] M.M. Siegel, K. Tabei, A. Kunz, I.J. Hollander, P.R. Hamann, D.H. Bell, S. Berkenkamp, F. Hillenkamp, Anal. Chem. 69 (1997) 2716.
[12] S.J. Lawson, K.K. Murray, Rapid Commun. Mass Spectrom. 14 (2000) 129.
[13] D. Twerenbold, A. Netuschill, N. de Rooij, P. Luginbuhl, D. Gerber, D. Gritti, Y. Gonin, F. Rossel, J.-L. Vuilleumier, Proteomics 2 (2002) 436.
[14] M. Bromirski, A. Loboda, W. Ens, K.G. Standing, in: Proceedings of the 48th ASMS Conference on Mass Spectrometry and Allied Topics, Long Beach, CA, 11–15 June 2000, p. 915.
[15] M. Bromirski, W. Ens, A. Loboda, K.G. Standing, S. Berkenkamp, F. Hillenkamp, in: Proceedings of the 49th ASMS Conference on Mass Spectrometry and Allied Topics, Chicago, IL, 27–31 May 2001.
[16] C. Menzel, K. Dreisewerd, S. Berkenkamp, F. Hillenkamp, Int. J. Mass Spectrom. 207 (2001) 73.
[17] K.L. Caldwell, D.R. McGarity, K.K. Murray, J. Mass Spectrom. 32 (1997) 1374.
[18] M. Sadeghi, Z. Olumee, X. Tang, A. Vertes, Z.X. Jiang, A.J. Henderson, H.S. Lee, C.R. Prasad, Rapid Commun. Mass Spectrom. 11 (1997) 393.
[19] J.D. Sheffer, K.K. Murray, Rapid. Commun. Mass Spectrom. 12 (1998) 1685.
[20] E.E. Durant, R.S. Brown, in: Proceedings of the 46th ASMS Conference on Mass Spectrometry and Allied Topics, Orlando, 31 May–4 June 1998, p. 929.
[21] R. Cramer, F. Hillenkamp, R.F. Haglund, J. Am. Soc. Mass Spectrom. 7 (1996) 1187.
[22] R. Cramer, R.F. Haglund, F. Hillenkamp, Int. J. Mass Spectrom. Ion Process. 169/170 (1997) 51.
[23] W.P. Hess, H.K. Park, O. Yavas, R.F. Haglund, Appl. Surf. Sci. 127–129 (1998) 235.
[24] M. Papantonakis, M. Baltz-Knorr, D. Ermer, R. F. Haglund, in: Proceedings of the 47th ASMS Conference on Mass Spectrometry and Allied Topics, Dallas, TX, 13–17 June 1999.
[25] V.L. Talrose, M.D. Person, R.M. Whittal, F.C. Walls, A.L. Burlingame, M.A. Baldwin, Rapid Commun. Mass Spectrom. 13 (1999) 2191.
[26] R.J. Keller, The Sigma Library of FR-IR Spectra, vols. 1 and 2, Sigma Chemical Company, 1988.
[27] C. Menzel, K. Dreisewerd, S. Berkenkamp, F. Hillenkamp, J. Am. Soc. Mass Spectrom. 13 (2002) 975.
[28] L.V. Zhigilei, B.J. Garrison, J. Appl. Phys. 88 (2000) 1281.
[29] L.V. Zhigilei, Y.G. Yingling, T.E. Itina, T.A. Schoolcraft, B.J. Garrison, Int. J. Mass Spectrom., this issue.
[30] M. Karas, M. Glückmann, J. Schäfer, J. Mass Spectrom. 35 (2000) 1.
[31] D. Feldhaus, C. Menzel, S. Berkenkamp, F. Hillenkamp, K. Dreisewerd, J. Mass Spectrom. 35 (2000) 1320.
[32] K. Dreisewerd, M. Schürenberg, M. Karas, F. Hillenkamp, Int. J. Mass Spectrom. Ion Process. 141 (1995) 127.
[33] S.L. Gournay, J. Acoust. Soc. Am. 40 (1966) 1322.
[34] C. Menzel, A. Rohlfing, A. Leisner, S. Berkenkamp, H. Ehring, L.M. Kukreja, F. Hillenkamp, K. Dreisewerd, in: Proceedings of the 49th ASMS Conference on Mass Spectrometry and Allied Topics, Chicago, IL, 27–31 May 2001.
[35] R.S. Dingus, R.J. Scammon, Proc. Laser–Tissue Interaction II 1427 (1991) 45.
[36] J.C. Miller, R.F. Haglund (Eds.), Laser Ablation, Mechanisms and Applications, Lecture Notes Phys., vol. 389, Springer, Berlin, 1991.
[37] M. von Allmen, Laser Beam Interactions with Materials, Springer Series in Material Sciences, vol. 2, Springer, Berlin, 1987.
[38] D. Kim, M. Ye, C.P. Grigoropoulos, Appl. Phys. A 67 (1998) 169.
[39] J.T. Walsh, J.P. Cummings, Lasers Surgery Med. 15 (1994) 295.
[40] E.D. Jansen, T.G. van Leeuwen, M. Motamedi, C. Borst, A.J. Welch, J. Appl. Phys. 78 (1995) 564.
[41] V. Venugopalan, N.S. Nishioka, B.B. Mikic, Biophys. J. 70 (1996) 2981.
[42] R. Kelly, A. Miotello, Phys. Rev. E 60 (1999) 2616.
[43] A. Oraevsky, S.L. Jacques, R.O. Esenaliev, F.K. Tittel, Lasers Surgery Med. 18 (1996) 231.
[44] G. Paltauf, H. Schmidt-Kloiber, Appl. Phys. A 62 (1996) 303.
[45] C.P. Lin, M.W. Kelly, Appl. Phys. Lett. 72 (1998) 2800.
[46] J. Sunner, Org. Mass Spectrom. 28 (1993) 805.
[47] R. Zenobi, R. Knochenmuss, Mass Spectrom. Rev. 17 (1998) 337.
[48] R. Knochenmuss, A. Stortelder, K. Breuker, R. Zenobi, J. Mass Spectrom. 35 (2000) 1237.
[49] B.H. Wang, K. Dreisewerd, U. Bahr, M. Karas, F. Hillenkamp, J. Am. Soc. Mass Spectrom. 4 (1993) 393.
[50] V. Bökelmann, B. Spengler, R. Kaufmann, Eur. Mass Spectrom. 1 (1995) 81.
[51] P. Arpino, Mass Spectrom. Rev. 9 (1990) 631.
[52] A.T. Iavarone, J.C. Jurchen, E.R. Williams, Anal. Chem. 73 (2001) 1455.
[53] K.A. Caldwell, M.L. Gross, J. Am. Soc. Mass Spectrom. 5 (1994) 72.
[54] J. Kampmeier, K. Dreisewerd, M. Schürenberg, K. Strupat, Int. J. Mass Spectrom. Ion Process. 169/170 (1997) 31.
[55] H. Ehring, PhD Thesis, University of Münster, 1993.
[56] S.F. Niu, W. Zhang, B.T. Chait, J. Am. Soc. Mass Spectrom. 9 (1998) 1.
[57] V. Horneffer, K. Dreisewerd, H.-C. Luedemann, F. Hillenkamp, M. Laege, K. Strupat, Int. J. Mass Spectrom. 185/186/187 (1999) 859.

[58] M.R. Papantonakis, J. Kim, W.P. Hess, R.F. Haglund, J. Mass Spectrom. 37 (2002) 639.
[59] S. Berkenkamp, C. Menzel, F. Hillenkamp, K. Dreisewerd, J. Am. Soc. Mass Spectrom. 13 (2002) 209.
[60] D.E. Ermer, M. Baltz-Knorr, R.F. Haglund, J. Mass Spectrom. 36 (2001) 538.
[61] S. Berkenkamp, C. Menzel, F. Hillenkamp, in: Proceedings of the 48th Conference on Mass Spectrometry and Allied Topics, Dallas, TX, 13–17 June 1999, p. 831.
[62] S. Berkenkamp, PhD Thesis, University of Münster, 2001.
[63] W.Z. Zhang, S.F. Niu, B.T. Chait, J. Am. Soc. Mass Spectrom. 9 (1998) 879.
[64] R. Cramer, A.L. Burlingame, Rapid Commun. Mass Spectrom. 14 (2000) 53.
[65] B.A. Budnik, K.B. Jensen, T.J.D. Jorgensen, A. Haase, R.A. Zubarev, Rapid Commun. Mass Spectrom. 14 (2000) 578.
[66] V.V. Laiko, N.I. Taranenko, V.D. Berkout, M.A. Yakshin, C.R. Prasad, H.S. Lee, V.M. Doroshenko, J. Am. Soc. Mass Spectrom. 13 (2002) 354.